Fracture-Controlled Mechanical Behavior of Steel Fiber-Reinforced Ultra-High-Performance Concrete Incorporating Slag and Limestone Powder Under Static and Impact Loading

Sci

Article

Fracture-Controlled Mechanical Behavior of Steel Fiber-Reinforced Ultra-High-Performance Concrete Incorporating Slag and Limestone Powder Under Static and Impact Loading

Roz-Ud-Din Nassar [1,*], Anagi Balachandra [2], Shah Room [3,*], Parviz Soroushian [4], Yang Chen [5,6] and Ali Bahadori-Jahromi [3]

1 Department of Architecture and Civil Engineering, American University of Ras Al Khaimah, Ras Al Khaimah, United Arab Emirates
2 Research Development, Michigan Engineering, University of Michigan, Ann Arbor, MI 48109-2102, USA; anagi4248@outlook.com
3 Department of Civil Engineering and Built Environment, School of Computing and Engineering, University of West London, London W5 5RF, UK; ali.bahadori-jahromi@uwl.ac.uk
4 Civil and Environmental Engineering Department, Michigan State University, East Lansing, MI 48824, USA; parvizsoroushian1@gmail.com
5 Department of Mechanical Engineering, University of Maryland, Baltimore, MD 21250, USA; yangchen@umbc.edu
6 Department of Computer Science and Electrical Engineering, University of Maryland, Baltimore, MD 21250, USA
* Correspondence: rozuddin.nassar@aurak.ac.ae (R.-U.-D.N.); shah.room@uwl.ac.uk (S.R.)

Abstract

Ultra-high-performance concrete (UHPC) is characterized by exceptional compressive strength; however, its structural performance is primarily governed by tensile behavior, fracture resistance, and energy dissipation. This study presents a comprehensive mechanical characterization of a steel fiber-reinforced UHPC incorporating a slag–limestone powder-based binder system with a low water-to-binder ratio of 0.15 and steam curing at 90 °C for 48 h. The experimental program comprised compressive strength, flexural behavior, split and direct tensile response, impact energy absorption, ultrasonic pulse velocity, and an assessment of specimen size and geometry effects. The UHPC achieved mean compressive strengths of approximately 209 and 218 MPa at 7 and 28 days, respectively, in 75 × 150 mm cylindrical specimens, indicating only modest strength development after the initial steam-curing period. Smaller cube specimens exhibited higher nominal compressive strengths, reaching approximately 221 and 227 MPa at 7 and 28 days, respectively, demonstrating a measurable but limited specimen-size effect. Flexural testing produced an average strength of 33.1 MPa and a stable post-peak response, although no strain hardening in bending was observed. Split tensile strength reached approximately 16.1 MPa, exceeding that of conventional normal-strength concrete by more than four times. Direct tensile tests demonstrated an intrinsically ductile response, with tensile strengths above 10.9 MPa and strain capacities of 0.25–0.30%, including a pronounced strain-hardening regime. Under drop-weight impact loading, specimens absorbed more than 40 J of energy without catastrophic fragmentation. Ultrasonic pulse velocity averaged 5344 m/s, indicating a dense and well-integrated microstructure. Overall, the results confirm that the investigated UHPC functions as a fracture-resistant structural composite in which tensile capacity, fiber-controlled crack bridging, and energy dissipation govern performance across multiple loading modes.

Check for updates

Academic Editors: Sanichiro Yoshida and Francesco Tajani

Received: 30 June 2026
Revised: 21 August 2026
Accepted: 3 September 2026
Published: 7 September 2026

Keywords: ultra-high-performance concrete; mechanical behavior; tensile ductility; fracture resistance; impact energy absorption

1. Introduction

UHPC is generally defined as a cementitious composite produced with very low water-to-binder ratios, typically 0.15–0.20, and dense particle packing, combined with steel fiber reinforcement [1]. Through the synergistic effects of matrix densification, pozzolanic reactions, and fiber bridging, UHPC achieves compressive strength levels that substantially exceed those of conventional and high-strength concretes. While conventional normal-strength concrete commonly exhibits compressive strengths below 50 MPa and high-strength concrete rarely exceeds 100–120 MPa [2], UHPC mixtures routinely achieve compressive strengths above 150 MPa, with values approaching or exceeding 200 MPa reported under controlled curing regimes such as steam curing at temperatures around 90 °C [3]. These strength levels are typically accompanied by bulk densities of 2.4–2.5 g/cm^3 and porosity values below approximately 3%, reflecting the extremely dense microstructure of UHPC.

Although its classification is mainly strength-based in practice, UHPC is increasingly recognized as a structural composite whose performance cannot be adequately described by compressive strength alone. Structural response in cement-based materials is governed primarily by tensile cracking, crack propagation, and post-cracking load transfer, particularly under service and ultimate limit states. In UHPC, the incorporation of steel fibers at volume fractions commonly ranging from 1.5% to 3.0% fundamentally alters the fracture process. Fiber bridging across cracks enables load transfer after matrix cracking, leading to ductile behavior and enhanced energy dissipation that are not observed in plain high-strength concretes, which often fail in a brittle manner once peak stress is reached [4].

Direct tensile strengths reported for steel fiber-reinforced UHPC generally range from 8 to 15 MPa, corresponding to roughly 5–10% of the compressive strength, whereas conventional concrete typically exhibits tensile strengths of only 2–4 MPa, representing less than 10% of its compressive capacity. This increase is not merely a function of matrix strength [5]. Still, it is strongly dependent on fiber–matrix bond characteristics, fiber aspect ratio, and the effective number of fibers intersecting the crack plane. UHPC mixtures exhibiting strain-hardening behavior have been reported to achieve tensile strain capacities exceeding 0.2–0.4%, compared with values on the order of 0.01% for normal-strength concrete [6]. However, many UHPC mixtures that do not achieve multiple cracking still display stable post-peak softening with significant residual stress [7,8]. This behavior remains structurally relevant but is often insufficiently documented through direct tensile testing.

Flexural performance provides a practical and widely adopted measure of UHPC ductility and fracture resistance, as bending tests capture both crack initiation and post-cracking load transfer. Flexural strengths reported for UHPC typically range from 10 to 40 MPa, depending on fiber content, fiber geometry, and curing conditions [9]. For comparison, the flexural strengths of normal-strength concrete are typically below 6 MPa, whereas fiber-reinforced high-strength concrete may reach 15–25 MPa. Significantly, UHPC flexural strength does not scale linearly with compressive strength. Two UHPC mixtures with similar compressive strengths may differ in flexural capacity by more than 50%, highlighting the dominant role of fiber reinforcement and crack-bridging efficiency [10,11]. Moreover, the shape of the load-deflection curve, including post-peak residual strength and total absorbed energy, is often more indicative of structural performance than peak flexural stress alone.

Impact resistance is another mechanical attribute in which UHPC exhibits substantial improvement over conventional concrete. Drop-weight impact tests reported in the literature indicate that UHPC can absorb several times more energy than normal-strength concrete of comparable dimensions [12], with measured impact energy absorption values frequently exceeding 30–50 J for thin UHPC plates, compared with values below 10 J for conventional concrete. This enhancement is attributed to distributed cracking, crack deflection, and fiber pull-out mechanisms that dissipate energy during rapid loading. Despite this, impact resistance is often treated as an isolated property, and few studies explicitly relate impact energy absorption to monotonic tensile or flexural behavior measured on the same UHPC mixture, limiting mechanistic interpretation [13,14].

The influence of specimen size and geometry on the measured compressive strength of UHPC introduces additional complexity. In conventional concrete, reducing specimen size from standard cylinders to smaller cubes can increase measured compressive strength by 10–25% due to statistical size effects and boundary conditions [15]. In UHPC, reported size effects are often more minor, frequently on the order of 5–15%, yet they remain non-negligible [16]. The presence of steel fibers is expected to reduce size sensitivity by enhancing crack bridging and energy dissipation; however, the degree of mitigation depends on fiber distribution and specimen geometry. Studies [17–19] comparing cube sizes of 50 mm and 75 mm, as well as cylinders with diameters between 75 and 100 mm, indicate that even in UHPC, measurable reductions in nominal strength occur with increasing specimen size. Given that laboratory testing of UHPC often relies on small specimens due to equipment limitations, understanding size effects is essential for interpreting reported compressive strength values and for establishing reliable conversion factors [20,21].

Non-destructive indicators such as ultrasound pulse velocity provide supplementary insight into the uniformity and internal integrity of UHPC. Typical pulse velocity values reported for UHPC exceed 4500–5000 m/s, compared with approximately 3500–4200 m/s for normal-strength concrete [22]. These elevated velocities reflect the dense granular skeleton, reduced connected porosity, and improved continuity of the solid phase that characterize UHPC. In particular, the refined pore structure reduces wave scattering and attenuation at void boundaries, enabling faster, more consistent transmission of ultrasonic waves through the material.

Beyond absolute velocity values, ultrasound pulse velocity measurements are especially useful for assessing specimen-to-specimen consistency within a test series. When specimens exhibit comparable pulse velocities, variations in mechanical response are more likely to be associated with testing variability or geometric effects rather than internal defects or material heterogeneity. This is particularly relevant when comparing specimens of different sizes or shapes, where differences in measured strength may otherwise be attributed to material inconsistencies. In this context, ultrasound measurements provide a qualitative means of verifying internal uniformity before or alongside destructive testing. While ultrasound pulse velocity cannot replace direct mechanical testing, it offers a valuable complementary metric for interpreting strength data and associated scatter [23].

These observations highlight a persistent gap in the UHPC literature. While compressive strengths above 150 MPa are widely reported, integrated datasets that simultaneously address tensile behavior, flexural response, impact resistance, and specimen-size effects within a single UHPC system remain limited. Many studies [24–26] investigate these properties independently, often using different mixtures, fiber contents, or curing regimes, making it difficult to establish quantitative relationships between strength, ductility, and fracture resistance. Given that UHPC behavior is directed by coupled mechanisms involving matrix densification, fiber bridging, and energy dissipation, a unified experimental framework is required to provide coherent mechanical interpretation [27,28].

The present study addresses this gap by conducting a comprehensive mechanical characterization of a steel fiber-reinforced UHPC formulated using a densely packed binder system comprising ordinary Portland cement, GGBFS, and limestone powder. The incorporation of slag and limestone powder was intended to develop a low-clinker, environmentally sustainable UHPC while maintaining exceptional mechanical performance. The experimental program includes compressive strength testing with statistical evaluation, flexural strength and load–deflection response, split tensile strength, direct tensile stress–strain behavior, drop-weight impact energy absorption, ultrasonic pulse velocity measurements, and an investigation of specimen size and shape effects on compressive strength. All tests were performed on specimens cast from the same fixed mixture composition and subjected to identical steam-curing conditions, thereby enabling direct comparison of the various mechanical responses. The study aims to quantify and interpret the mechanical performance, ductility, and fracture behavior of a sustainable slag–limestone powder-based UHPC beyond compressive strength alone, with particular emphasis on tensile resistance, energy absorption capacity, and size-dependent strength characteristics. By integrating a broad spectrum of mechanical performance indicators within a single experimental framework, this work provides a comprehensive assessment of the structural behavior of a low-clinker UHPC and contributes to a deeper mechanics-based understanding of its strength, toughness, and deformation capacity.

2. Experimental Program

2.1. Materials

The ultra-high-performance concrete investigated in this study was produced using commercially available constituents selected to achieve a densely packed granular skeleton and superior mechanical performance. Crushed limestone aggregate (No. 8) and ground granulated blast furnace slag (Newcem 100) were supplied by Builder Redi-Mix Concrete Corporation, Lansing, MI, USA. Ordinary Portland cement (Type I) and silica sand (FS #52) were procured from a local supplier. Limestone powder and silica fume were obtained from Duda Energy, LLC, Decatur, AL, USA. A polycarboxylate ether-based high-range water-reducing admixture (Chryso 150) was used to achieve the required workability at a very low water-to-binder ratio.

Straight steel fibers supplied by Bekaert Corporation, US-Orrville, OH, USA, with a nominal length of 15 mm, diameter of 0.5 mm, and aspect ratio of 30, were incorporated into the mixture. The fibers possess a nominal tensile strength of approximately 2800 MPa and an elastic modulus of 210 GPa, consistent with typical values for low-carbon steel fibers. The fibers were added at a dosage of 117.9 kg/m^3, corresponding to a volume fraction of approximately 1.5%. The fresh UHPC mixture exhibited a target slump of 265 mm, providing adequate workability for casting despite the low water-to-binder ratio and fiber incorporation. All materials were used as received without further treatment.

2.2. Mix Design

The UHPC mixture was proportioned to achieve a highly compacted matrix with low porosity and enhanced mechanical performance. The mix design is summarized in Table 1 and corresponds to a total aggregate content of approximately 1270 kg/m^3, composed of coarse limestone aggregate and fine silica sand. The binder system consisted of Portland cement, silica fume, slag, and limestone powder, resulting in a total cementitious content exceeding 950 kg/m^3. The water-to-binder ratio was fixed at 0.15 to limit capillary porosity and promote high matrix strength. A high dosage of superplasticizer was employed to compensate for the reduced water content and to maintain sufficient workability for casting.

https://doi.org/10.3390/sci8090248

The dosage of steel fibers was selected to enhance tensile strength, crack-bridging capability, and post-cracking behavior of the UHPC.

Table 1. Mix design for evaluation of the effect of fiber fraction.

Materials	kg/m^3
Total Aggregates	1270.161
Coarse Aggregate	482.661
Silica sand	787.661
Cement	476.31
Silica fume	209.577
Slag	95.262
Limestone powder	171.472
Water	123.646
HWRA (31%) Chryso 150	44.297
Steel fiber	117.900

To ensure a clear and consistent assessment of fiber-related effects, single UHPC mixture was adopted throughout the study. Maintaining a constant matrix composition enabled the influence of steel fiber characteristics on the mechanical and impact performance to be isolated without introducing additional variability associated with changes in the binder system or mixture proportions.

2.3. Mixing, Casting, and Curing Procedures

Mixing was carried out using a controlled sequence to ensure uniform dispersion of constituents and steel fibers. All dry materials, including aggregates, cement, silica fume, slag, and limestone powder, were first blended at low speed (approximately 140 rpm) for 2 min to achieve a homogeneous mixture. Subsequently, water premixed with the superplasticizer was added gradually, followed by the remaining water, while mixing continued at medium speed (approximately 285 rpm) for 4 min until a cohesive mixture was obtained.

Steel fibers were then introduced slowly over a period of approximately 2 min at low speed to minimize fiber agglomeration, followed by an additional 2 min of mixing at medium speed to ensure uniform dispersion. The total mixing duration from the initial water addition was approximately 12 min.

The fresh UHPC mixture was cast into steel molds corresponding to the required specimen geometries for mechanical testing. After casting, the specimens were covered with a wet cloth and stored at room temperature for 24 h. Following demolding, they were steam-cured at 90 °C for 48 h to accelerate hydration and pozzolanic reactions, thereby promoting the dense microstructure and high early-age strength characteristic of UHPC. During steam curing, the temperature was increased at an approximate rate of 2–3 °C/min until the target temperature was reached and maintained, while relative humidity was kept above 95% to prevent moisture loss. After completion of the curing cycle, specimens were allowed to cool gradually within the chamber to ambient temperature to minimize thermal shock. This approach is commonly adopted for mixtures with low water-to-binder ratios and supplementary cementitious materials such as slag. Subsequently, the specimens were conditioned at approximately 50% relative humidity until the designated testing age to ensure consistent material development and minimize variability in their mechanical response.

3. Experimental Procedures

The experimental program was designed to characterize the mechanical performance, ductility, and size-dependent behavior of the UHPC mixture under quasi-static and impact loading. The investigation focused on compressive strength, flexural strength, and load–deflection response, split tensile strength, direct tensile behavior, impact energy absorption, ultrasound pulse velocity, and specimen size effects on compressive strength. All specimens were produced from the same batch proportions and subjected to identical curing conditions to ensure consistency across tests.

Except for compressive strength, which was evaluated at 7 and 28 days, all mechanical properties were measured at 7 days. Three replicate specimens were tested for each property at each specified age, and the reported values represent the corresponding mean measurements. Confidence intervals, where presented, were calculated from the replicate results.

3.1. Bulk Density, Water Absorption, and Void Content

Three replicate specimens were tested, and the reported values represent the mean of the three measurements. The specimens were oven dried at 110 °C for a minimum of 24 h until a constant mass was achieved and then cooled to room temperature in a desiccator. The oven-dried specimens were subsequently immersed in water at 21 °C for 48 h, after which the saturated surface-dry mass was determined. The specimens were then boiled in water for 5 h and allowed to cool in water for 14 h before a second saturated surface-dry mass was measured. Finally, the apparent mass of each specimen was determined while suspended in water using a thin wire. The bulk density, water absorption, and void content were calculated in accordance with the procedures and equations specified in ASTM C642 [29].

3.2. Compressive Strength

Compressive strength tests were conducted at 7 and 28 days using 75 mm × 150 mm UHPC cylindrical specimens. This specimen geometry was selected to provide a larger and more representative basis for evaluating the compressive strength of the investigated UHPC mixture and to facilitate comparison with cylinder-based strength data reported in the literature. Testing was performed using a Matest compression testing machine (Matest, Treviolo, Italy) under monotonic loading as shown in Figure 1A. The tests were carried out under displacement control, with a loading rate corresponding to a stress increase of approximately 0.25 MPa/s until failure. The compressive strength was calculated by dividing the maximum load at failure by the nominal cross-sectional area. The failure mode was observed to be non-brittle, characterized by distributed cracking and confinement effects associated with the presence of steel fibers.

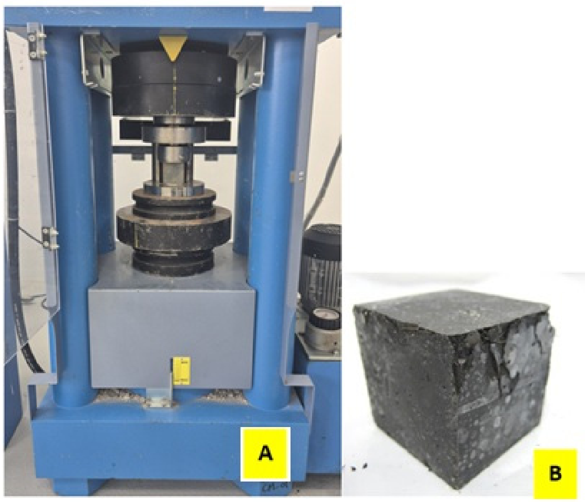

Figure 1. Compression test setup (**A**), and a UHPC specimen after failure in compression (**B**).

To evaluate size and geometry effects, compressive strength tests were performed on specimens of varying dimensions and shapes, including 50 mm cubes, 75 mm cubes (Figure 1B) and 75 mm × 150 mm cylinders. For each configuration, three specimens were tested, and the results are presented as mean values with corresponding variability. Larger cylindrical specimens (100 mm × 200 mm) were also prepared; however, these could not be tested due to equipment capacity limitations. The influence of specimen size and geometry on nominal compressive strength was assessed by comparing the mean values and their associated confidence intervals.

3.3. Flexural Strength and Load–Deflection Behavior

Flexural performance was evaluated using four-point bending test (Figure 2A) conducted in accordance with ASTM C78 [30]. Prismatic specimens measuring 285 mm × 50 mm × 50 mm were tested (Figure 2B). Load was applied under displacement control, and the applied load and mid-span deflections were recorded using a calibrated load cell and two linear variable displacement transducers (LVDTs). The load–deflection response was used to evaluate flexural strength, post-cracking behavior, and ductility. Failure was characterized by stable crack development and sustained load transfer facilitated by fiber bridging.

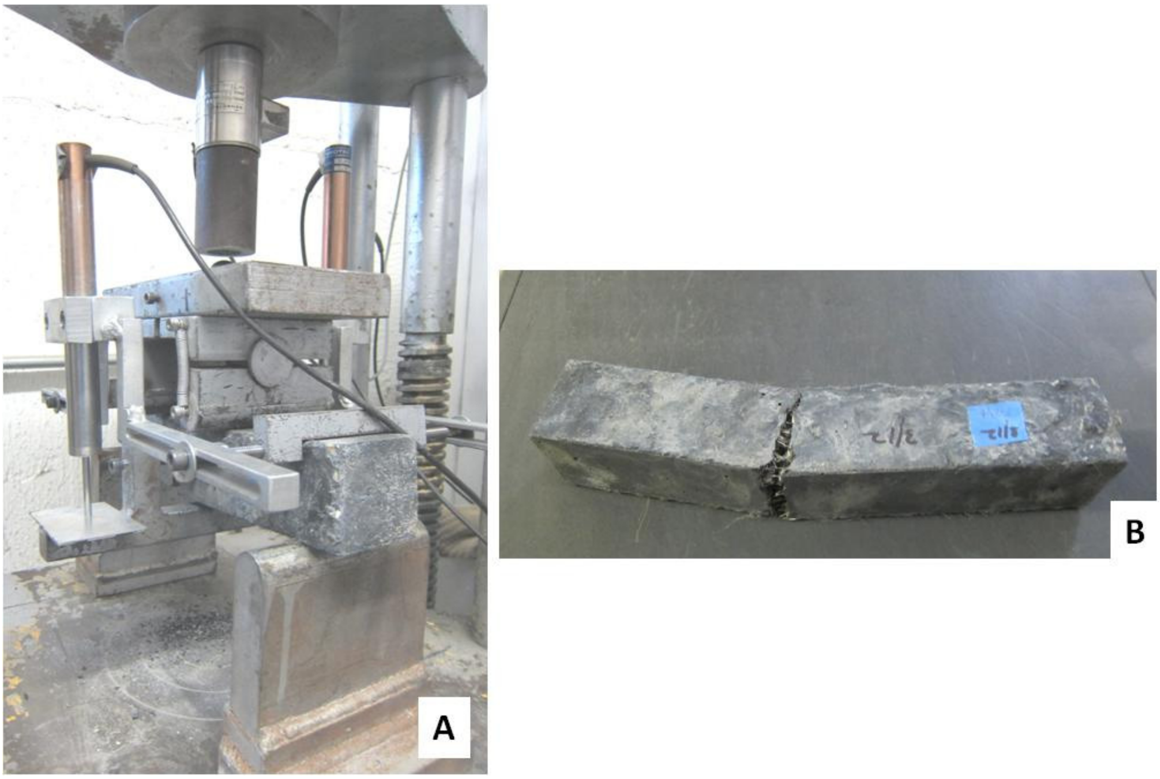

Figure 2. Flexure test setup (**A**), and a failed flexure test specimen (**B**).

3.4. Split Tensile Strength

Split tensile strength was measured following ASTM C496 [31] using cylindrical specimens with a diameter of 76 mm and a height of 152 mm (Figure 3). Diametral compressive loading was applied until failure, and the split tensile strength was calculated from the peak load. The specimens exhibited distributed cracking and ductile failure behavior due to the restraining effect of steel fibers.

Figure 3. Split tension test setup.

3.5. Direct Tensile Strength and Load–Deformation Behavior

Direct tensile tests were performed on prismatic UHPC specimens with a square cross section of 50 mm × 50 mm and a total length of 290 mm (Figure 4A). The tests were conducted using a dedicated tensile testing setup designed to ensure axial alignment of the applied load and minimize load eccentricity (Figure 4B). Tensile loading was applied under displacement-controlled conditions. The applied load was measured using a calibrated load cell, while axial deformation was recorded using two displacement transducers mounted symmetrically on opposite faces of the specimen over the central gauge region. The average deformation recorded by the two transducers was used to determine the axial strain, and the corresponding tensile stress was calculated by dividing the applied load by the nominal cross-sectional area of the specimen. The use of a dedicated tensile loading fixture together with symmetrical deformation measurements minimized eccentricity and end effects, thereby promoting predominantly uniaxial tensile loading. The resulting tensile stress–strain response was used to evaluate the direct tensile strength, post-peak behavior, and deformation capacity of the UHPC.

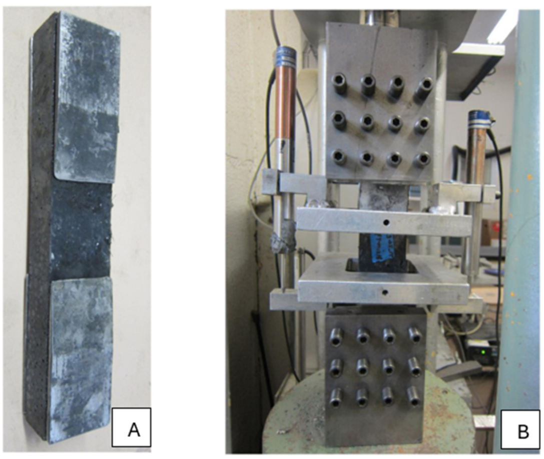

Figure 4. Direct tension: (**A**) Test specimen. (**B**) Test setup.

3.6. Impact Resistance

Impact resistance was assessed per ASTM D7136 [32] using a drop-weight impact testing system (Figure 5A,B) with a maximum capacity of 260 J. Prismatic specimens measuring 140 mm × 140 mm × 20 mm were tested (Figure 6A,B). Three replicate specimens were tested for each mixture. The specimens were rigidly clamped along all four edges, and a 7.82 kg steel impactor fitted with a hemispherical striking head of 10 mm radius was released from a predetermined height to impact the center of the specimen. Impact force was continuously recorded using a calibrated load cell connected to a high-speed data acquisition system.

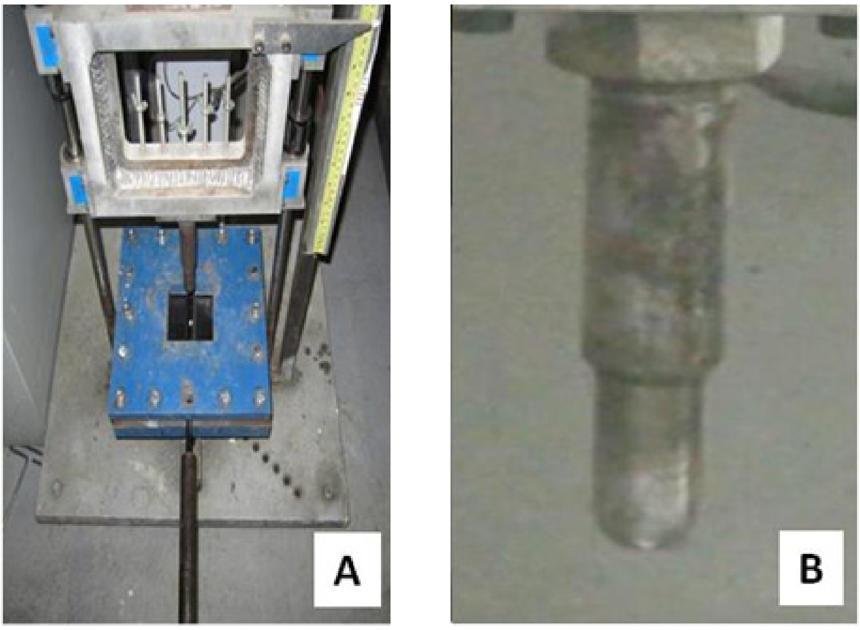

Figure 5. Drop-weight impact test setup (**A**), and hemispherical loading tip (**B**).

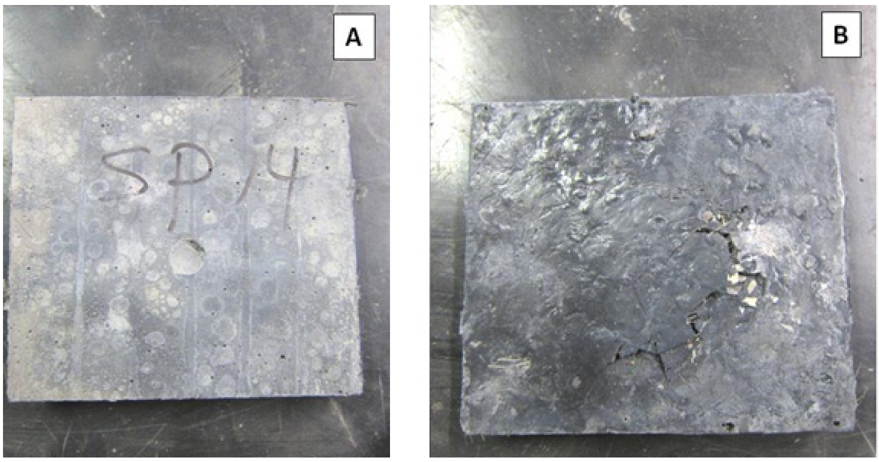

Figure 6. A UHPC specimen after impact testing: (**A**) front face, (**B**) back surface.

The absorbed impact energy was determined from the measured force–time history using the energy-balance relationships expressed in Equations (1) and (2). The absorbed energy was defined as the reduction in the kinetic energy of the impactor during the impact event. Specimen failure was identified by the occurrence of severe cracking and a substantial loss of load-carrying capacity following impact, as confirmed from the recorded force–time response and post-impact visual inspection.

$$E_{ab}(t) = \frac{mv_0^2}{2} - \frac{m[v_t]^2}{2} \quad (1)$$

$$v_t = v_o - \frac{1}{m}\int_0^t F.dt \quad (2)$$

In the above equation, $E_{ab}(t)$ is the total absorbed energy (J), m is the drop-weight mass (kg), v_o is the initial velocity (m/s), t is the time after impact (s), v_t is the velocity at time t after impact (m/s), and F is the force measured over time using a load cell. Representative front and rear views of an impacted specimen are presented in Figure 6. The high toughness imparted by the steel fibers contributed to the superior impact resistance of the UHPC.

3.7. Ultrasound Pulse Velocity

Ultrasound pulse velocity measurements were conducted to assess the internal uniformity and integrity of the UHPC specimens. The tests were performed on cylindrical specimens with a diameter of 75 mm and a height of 150 mm using a Proceq Pundit ultrasonic pulse velocity tester (Proceq, Schwerzenbach, Switzerland) shown in Figure 7.

Figure 7. The ultrasound pulse velocity test setup.

The measurements were carried out using the direct transmission method, in which the transmitting and receiving transducers were placed on opposite faces of the specimen along its longitudinal axis. A coupling gel was applied to ensure proper acoustic contact between the transducers and the specimen surfaces. For each specimen, the transit time of the ultrasonic pulse was recorded, and the pulse velocity was calculated as the ratio of the specimen length to the measured transit time.

Ultrasound pulse velocity was used as a non-destructive indicator of material uniformity and internal integrity. The measured values were compared with those obtained from normal-strength concrete specimens tested under identical conditions to provide a qualitative reference. While ultrasound pulse velocity does not replace mechanical testing, it provides supplementary information that aids in interpreting strength variability and assessing specimen consistency before destructive testing.

3.8. Size and Geometry Effects on Compressive Strength

To examine the effect of specimen size and geometry on compressive strength, UHPC specimens with different dimensions and shapes were prepared, as shown in Figure 8. Four specimen configurations were considered: (i) 50 mm cubes, (ii) 75 mm cubes, (iii) 75 mm × 150 mm cylindrical specimens, and (iv) 100 mm × 200 mm cylindrical specimens.

Figure 8. UHPC compression test specimens of different sizes and shapes.

Compressive strength tests were conducted on the 50 and 75 mm cubes and the 75 mm × 150 mm cylinders at 7 and 28 days. The 100 mm × 200 mm cylindrical specimens were fabricated but could not be tested because the load required to reach failure was beyond the capacity of the available compression testing machine. Consequently, these specimens were excluded from the comparative analysis. For each tested configuration and age, three replicate specimens were tested, and the results are reported as mean values with corresponding confidence intervals. The influence of specimen size and geometry on nominal compressive strength was assessed by comparing the mean strengths obtained for the different specimen configurations.

4. Results and Discussion

4.1. Bulk Density, Water Absorption, and Void Content

The bulk density, water absorption, and void content of the UHPC are summarized in Table 2. The UHPC exhibited a relatively high bulk density together with very low water absorption and void content, reflecting the highly compact and refined internal microstructure of the material. These characteristics can be attributed to the dense particle packing achieved through the carefully proportioned mixture design, the incorporation of supplementary cementitious materials (ground granulated blast furnace slag, limestone powder, and silica fume), and the very low water-to-binder ratio. The resulting reduction in pore volume and improvement in matrix continuity contribute not only to the high mechanical strength of the UHPC but also to its enhanced durability by limiting the ingress of water and other aggressive agents.

Table 2. Bulk density, water absorption, and void content of UHPC.

Bulk Density (g/cm^3)	Water Absorption Capacity (%)	Void Content (%)
2.472	0.903	2.23

4.2. Compressive Strength

The compressive strength development of the UHPC was evaluated at 7 and 28 days using 75 × 150 mm cylindrical specimens, and the results are presented in Figure 9. The mean compressive strength was approximately 209 MPa at 7 days and increased slightly to 218 MPa at 28 days. Thus, the average compressive strength exhibited only a modest increase of approximately 4% over the 21-day period following the initial 7-day testing age. This limited strength development is attributed primarily to the adopted curing and conditioning regime. Following 48 h of steam curing at 90 °C, the specimens were conditioned at room temperature and approximately 50% relative humidity until testing. Under these relatively dry conditions, the availability of external moisture for continued cement hydration and supplementary cementitious material reactions is limited, thereby restricting further strength development after the initial steam-curing period.

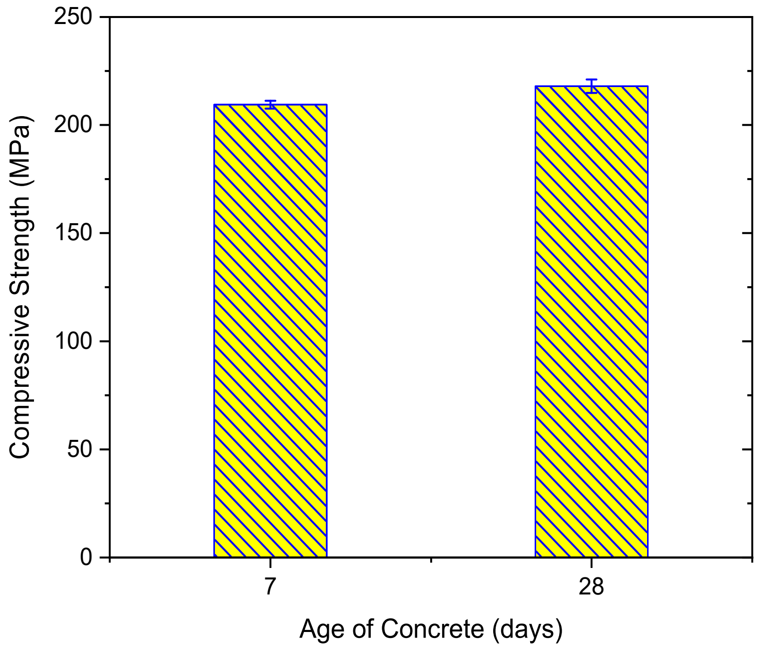

Figure 9. Mean compressive strength of UHPC at 7 and 28 days obtained from 75 × 150 mm cylindrical specimens.

The relatively small variation in the measured strengths, as indicated by the error bars in Figure 9, demonstrates good repeatability of the compressive strength measurements. This consistency can be attributed to the controlled mixing, casting, and curing procedures adopted in the study despite the very low water-to-binder ratio and high cementitious content of the UHPC mixture. The 28-day compressive strength of 218 MPa confirms the development of a highly dense and mechanically robust cementitious matrix.

The failure mode observed during compressive testing was non-brittle and characterized by distributed cracking and progressive damage rather than sudden catastrophic fracture. This behavior differs from the abrupt failure commonly observed in plain high-strength concrete. Although the compressive strength of UHPC is primarily governed by matrix density and strength, the presence of steel fibers can contribute to crack arrest and internal restraint, particularly at high stress levels where lateral dilation and microcrack development become increasingly important [33].

Table 3 places the compressive strength of the investigated UHPC in the context of representative values reported for normal-strength concrete, high-strength concrete, and UHPC. The normal-strength concrete produced in this project exhibited a compressive strength of approximately 48 MPa, which falls within the typical range reported for structural concrete. Reported compressive strengths of high-strength concrete generally extend from approximately 54 MPa to 120–130 MPa [34–36], depending on mixture composition and curing conditions. In comparison, compressive strengths reported for UHPC commonly extend to approximately 200 MPa, although higher values have also been reported depending on mixture composition, specimen geometry, and curing regime [37–40].

The 28-day compressive strength of 218 MPa obtained from the 75 × 150 mm cylindrical specimens places the investigated mixture at the upper end of the compressive strength range commonly reported for UHPC. This high strength can be attributed to the combined effects of the very low water-to-binder ratio of 0.15, high cementitious content, incorporation of reactive supplementary cementitious materials, dense particle packing, and steam curing at 90 °C for 48 h. The elevated curing temperature promotes accelerated hydration and pozzolanic reactions, resulting in rapid development and densification of the cementitious matrix [41].

The compressive strength results presented in this section represent the principal strength measurements of the investigated UHPC based on the 75 × 150 mm cylindrical specimens. The influence of specimen size and geometry, including the compressive strengths obtained from 50 and 75 mm cube specimens, is considered separately in Section 4.7. This separation allows the intrinsic strength development of the investigated mixture to be distinguished from variations in nominal strength associated with specimen dimensions and geometry.

Overall, the investigated UHPC achieved a mean compressive strength of approximately 209 MPa at 7 days and 218 MPa at 28 days under the adopted steam-curing and subsequent conditioning regime. The relatively limited increase in strength between the two ages indicates that most of the strength development occurred during the initial steam-curing period, while the subsequent conditioning at approximately 50% relative humidity provided limited moisture availability for further hydration. The high compressive strength and relatively low variability observed in the cylindrical specimens demonstrate the effectiveness of the adopted mixture and curing regime in producing a dense and mechanically robust UHPC matrix.

Table 3. Compressive strength test results for ultra-high-performance concrete (UHPC), normal-strength concrete, and high-strength concrete.

Concrete Type	Compressive Strength, MPa	Source
Normal-Strength	47.8	This Project
Normal-Strength	24.0–56.6	[42]
High-Strength	53.9–127	[43]
UHPC	218	This Project
UHPC	150–206	[44]
UHPC	132–180	[45]

4.3. Flexural Strength and Load–Deflection Behavior

The flexural response of the UHPC mixture was evaluated using four-point bending tests, and representative load–deflection and stress–deflection curves are shown in Figure 10A and 10B, respectively. The results demonstrate a distinctly ductile flexural behavior, characterized by a gradual reduction in load-carrying capacity after attaining the peak load rather than abrupt post-peak collapse. After first cracking, the specimens sustained significant additional deformation, with measurable load resistance maintained over deflections exceeding 10 mm, corresponding to several times the deflection at peak load. This behavior reflects effective crack bridging by the steel fibers, which limits crack opening and delays localization. The mean flexural strength of the UHPC mixture was 33.11 MPa, with a 95% confidence interval of ±2.72 MPa. Expressed in relative terms, the scatter in flexural strength corresponds to approximately 8% of the mean value, which is reasonable for fiber-reinforced systems where local fiber orientation and dispersion strongly influence bending performance. By comparison, flexural strength variability reported for conventional and high-strength concretes often exceeds 10%, particularly in the absence of fiber reinforcement [46]. The consistency observed here indicates stable mechanical performance despite the very high matrix strength and fiber content [47,48].

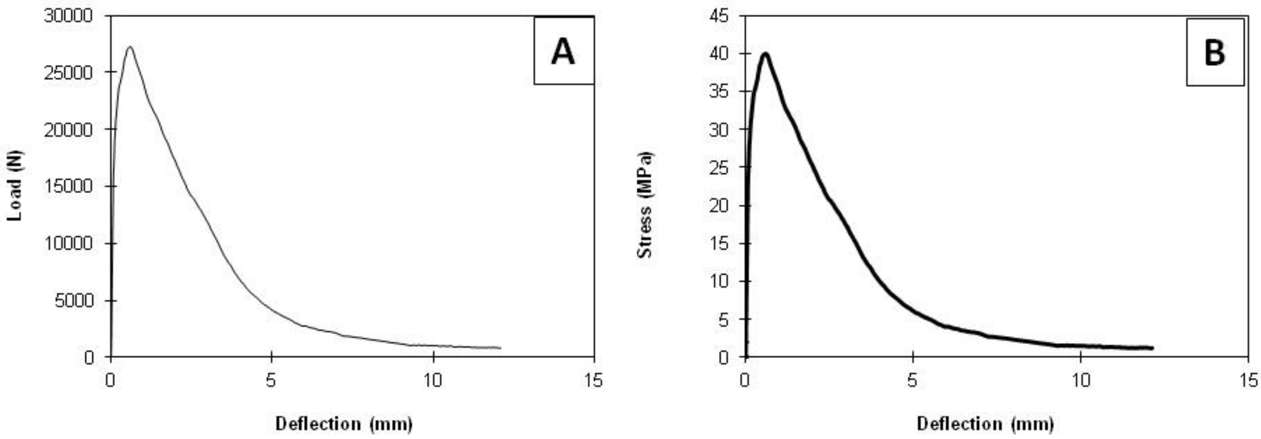

Figure 10. Representative flexural load–deflection (**A**) and corresponding stress–deflection (**B**) responses of UHPC, illustrating peak behavior and post-peak softening governed by fiber bridging.

Despite the high flexural strength, the UHPC mixture did not exhibit strain-hardening behavior in flexure. The load–deflection curves show a single dominant peak followed by stable softening, rather than a secondary rise in load associated with multiple cracking. This indicates that the flexural cracking strength of the matrix was not sufficiently lower than the adequate fiber bridging capacity to enable strain hardening [49,50]. In quantitative terms, the absence of a post-cracking strength increase suggests that the ratio between fiber bridging stress and matrix cracking stress remained below the threshold required for multiple crack formation, even though fiber content was sufficient to provide substantial post-peak load transfer. The post-peak response remains structurally significant. Following peak load, the flexural stress decreased gradually to residual levels on the order of a few megapascals, indicating that a non-negligible fraction of the peak load-carrying capacity was retained over large deflections. This corresponds to a flexural strength retention of 10–15% at large deflections, reflecting progressive fiber pull-out and debonding rather than sudden fiber rupture or matrix crushing [33,51]. Such behavior is associated with enhanced energy absorption and improved damage tolerance compared with brittle cementitious materials.

Table 4 presents the flexural strength results from this study alongside values reported for different concrete classes. The UHPC flexural strength of approximately 33 MPa is nearly three times greater than that of the plain normal-strength concrete produced in this project, which exhibited a flexural strength of about 11.8 MPa. Compared with typical literature values for normal-strength concrete, which commonly range from 4 to 7 MPa [52], the enhancement provided by the UHPC matrix and fiber reinforcement corresponds to roughly a 400–600% increase. Fiber-reinforced high-strength concrete, by contrast, typically achieves flexural strengths of 25–30 MPa, placing the present UHPC mixture at the upper end of that range [53,54]. When considered relative to compressive strength, the flexural strength of the UHPC mixture represents approximately 15% of the mean compressive strength of about 220 MPa. This ratio is substantially higher than that observed for normal-strength concrete, where flexural strength rarely exceeds 8–10% of compressive strength [5]. The higher flexural-to-compressive strength ratio highlights the role of fiber reinforcement in enhancing tensile stress transfer and crack resistance, despite the mixture was not specifically designed to promote strain-hardening behavior.

Table 4. Flexural strength values obtained in this project and reported in the literature for plain normal-strength concrete, fiber reinforced high-strength concrete, and UHPC.

Concrete Type	Flexural Strength, MPa	Source
Normal Strength	11.8	This Project
Normal Strength	4.05–6.53	[42]
Fiber Reinforced High Strength	28.5	[55]
UHPC	33.1	This Project
UHPC	16–44	[56]

4.4. Split Tensile Strength

The split tensile strength results for the UHPC mixture are summarized in Table 5, along with representative values reported in the literature for plain normal-strength concrete, plain high-strength concrete, and fiber-reinforced high-strength concrete. The UHPC specimens tested in this study exhibited a mean split tensile strength of 16.14 MPa, with a 95% confidence interval of ±0.92 MPa. In relative terms, this corresponds to approximately 6% variability around the mean, indicating a high degree of consistency despite the inherent sensitivity of tensile-dominated tests to local material heterogeneity and fiber distribution. Compared with the plain normal-strength concrete produced in this project, which exhibited a split tensile strength of approximately 3.9 MPa, the UHPC mixture demonstrates an increase in split tensile capacity by a factor exceeding 4. Compared with typical literature values for plain normal-strength concrete, which generally range from 2 to 4 MPa, the enhancement provided by UHPC corresponds to a 300–500% increase. This substantial improvement reflects both the high intrinsic tensile strength of the dense UHPC matrix and the contribution of steel fibers in restraining crack opening under indirect tensile loading [27,57].

Plain high-strength concrete reported in the literature typically exhibits split tensile strengths of 5–6 MPa, representing only a modest increase over normal-strength concrete when fiber reinforcement is absent. The incorporation of fibers into high-strength concrete increases the split tensile strength to approximately 7–12 MPa [58,59], depending on fiber content and geometry. The UHPC split tensile strength measured in this study exceeds the upper bound of fiber-reinforced high-strength concrete by approximately 30–40%, highlighting the combined effect of fiber reinforcement and matrix densification in UHPC systems. It is also helpful to consider the split tensile strength relative to the compressive strength. For the UHPC mixture investigated here, the split tensile strength of approximately 16 MPa corresponds to about 7–8% of the mean compressive strength of roughly 220 MPa [47,60]. This ratio is notably higher than that typically observed in normal-strength concrete, where split tensile strength rarely exceeds 5–6% of compressive strength. The elevated tensile-to-compressive strength ratio further highlights the role of fibers in enhancing tensile stress transfer and mitigating the inherent brittleness associated with very high matrix strength.

The failure mode observed during split tensile testing was ductile and characterized by distributed cracking rather than a single dominant fracture plane. While the Brazilian splitting test does not provide a pure tensile stress state, it offers valuable insight into the material's resistance to crack initiation and propagation under tensile-dominated loading. In UHPC, fiber bridging across the developing crack plane delays crack widening and enables sustained load transfer beyond first cracking, leading to higher measured split tensile strengths and reduced brittleness compared with plain concretes.

The comparison between UHPC and fiber-reinforced high-strength concrete is particularly revealing. Although both material classes benefit from fiber reinforcement, the markedly higher split tensile strength of UHPC indicates that its dense, refined matrix enhances the effectiveness of the fibers. Improved fiber–matrix bond, reduced interfacial defects, and limited capillary porosity contribute to more efficient stress transfer from the matrix to the fibers, allowing a greater fraction of the fiber bridging capacity to be mobilized under tensile loading [57,59,61].

The split tensile-strength results confirm that the UHPC mixture developed in this study exhibits tensile resistance that clearly distinguishes it from both normal-strength and conventional high-strength concretes, including those with fiber reinforcement [62]. The magnitude and consistency of the split tensile strength provide a quantitative link between the flexural ductility discussed in the previous section and the direct tensile behavior examined in the following section, reinforcing the interpretation of UHPC as a structural composite governed by enhanced tensile capacity and crack-bridging mechanisms rather than compressive strength alone.

Table 5. Split tensile strengths of UHPC versus plain normal-strength concrete, and plain and fiber-reinforced high-strength concrete.

Concrete Type	Split Tensile Strength, MPa	Source
Plain Normal-Strength	3.89	This Project
Plain Normal-Strength	2.14–3.83	[42]
Plain High-Strength	5.8	[63]
Fiber Reinforced High-Strength	6.9–11.9	[63]
UHPC	16.14	This Project
UHPC	11.3–23.8	[56]

4.5. Tensile Strength and Load–Deformation Behavior

The direct tensile response of the UHPC mixture was characterized through uniaxial tension tests, and representative load–deflection and stress–strain curves are shown in Figure 11A and 11B, respectively. Unlike indirect tensile methods, direct tension provides direct insight into crack initiation, crack evolution, and post-cracking stress transfer mechanisms. The UHPC specimens exhibited a mean tensile strength of 10.92 MPa, with a narrow 95% confidence interval of ±0.23 MPa, corresponding to a relative variability of approximately 2%. This limited scatter indicates a highly reproducible tensile response, despite the sensitivity of direct tensile testing to alignment, gripping conditions, and local fiber distribution [64].

The tensile stress–strain response is marked by an apparent deviation from linearity at relatively low strain levels, followed by a progressive increase in stress beyond first cracking. Peak tensile stress was attained at strain levels on the order of 0.25–0.30%, which is more than an order of magnitude greater than the tensile strain capacity of plain normal-strength concrete, typically limited to approximately 0.01–0.02% [65]. This extended strain capacity reflects the activation of fiber-bridging mechanisms following matrix cracking, enabling stress redistribution and delayed localization.

In contrast to the flexural response discussed previously, the tensile curves display a distinct strain-hardening phase, evidenced by a gradual increase in stress after initial cracking rather than an immediate transition to softening [66]. This behavior indicates that, under uniaxial tensile loading, the effective fiber bridging stress exceeded the matrix cracking stress over a finite strain interval. The occurrence of strain hardening in direct tension, even though it was not observed in flexure, highlights the sensitivity of UHPC cracking behavior to the imposed stress state and crack kinematics [67]. In bending, crack localization and stress gradients limit the development of multiple cracking. In contrast, the more uniform stress field in direct tension allows more effective mobilization of fiber bridging across the crack plane.

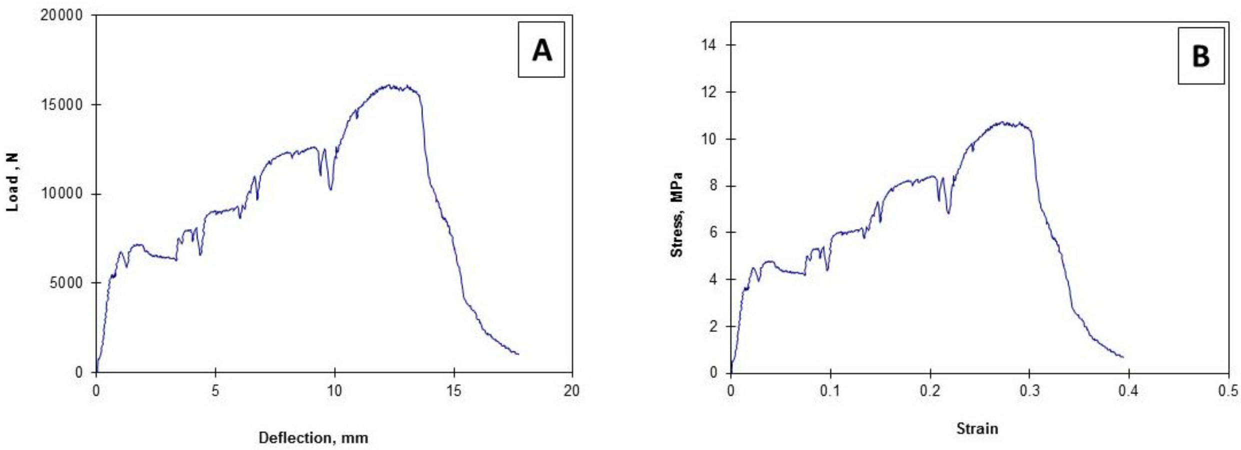

Figure 11. Typical tensile load-deflection (**A**) and stress–strain (**B**) behavior of UHPC.

The load–deflection curves further reveal a gradual reduction in load beyond the peak stress, with load resistance maintained over deflections approaching 15–18 mm. This post-peak response is governed by progressive fiber pull-out and interfacial debonding rather than abrupt fiber rupture, resulting in a controlled softening regime. Residual tensile stress levels of several megapascals were sustained at large strains, corresponding to a retention of roughly 20–30% of the peak tensile stress [40]. Such behavior is indicative of substantial tensile toughness and energy dissipation capacity.

Table 6 compares the tensile strength of the UHPC mixture with values reported for plain normal-strength concrete. The tensile strength of approximately 10.9 MPa obtained in this study exceeds typical normal-strength concrete tensile strengths, which generally range from about 1.6 to 2.5 MPa, by a factor of more than four. This enhancement cannot be attributed solely to increased matrix strength [24,68]. Instead, it reflects the combined influence of fiber reinforcement, improved fiber–matrix bond, and the refined microstructure of the UHPC matrix, which limits premature microcracking and enables efficient stress transfer to the fibers.

Table 6. Tensile strengths of plain normal-strength concrete and UHPC.

Concrete Type	Tensile Strength, MPa	Source
Normal-Strength	1.61–2.49	[42]
UHPC	10.9	This Project

When considered in relation to compressive strength, the direct tensile strength of the UHPC mixture corresponds to approximately 5% of the mean compressive strength. While this ratio is lower than that observed for flexural strength, it is significantly higher than the tensile-to-compressive strength ratio typical of normal-strength concrete. The difference between tensile and flexural strength ratios further highlights the role of stress state and crack geometry in governing the mobilization of fiber reinforcement. The direct tensile results provide a critical reference point for interpreting both the flexural and split tensile behaviors reported earlier. The presence of strain hardening and extended deformation capacity in direct tension confirms that the UHPC mixture possesses an intrinsically ductile tensile response, even though this ductility manifests differently under bending and indirect tensile loading [69,70]. This distinction highlights the importance of direct tensile testing to capture the fundamental tensile mechanics of UHPC and avoid reliance on indirect indicators alone.

4.6. Impact Energy Absorption

The impact response of the UHPC mixture was evaluated using drop-weight testing, and representative impact load–time histories, along with the corresponding cumulative energy absorption curves, are shown in Figure 12. Unlike quasi-static mechanical tests, the impact response reflects the material's ability to resist rapid load application, redistribute stresses over very short time scales, and dissipate kinetic energy through progressive damage mechanisms.

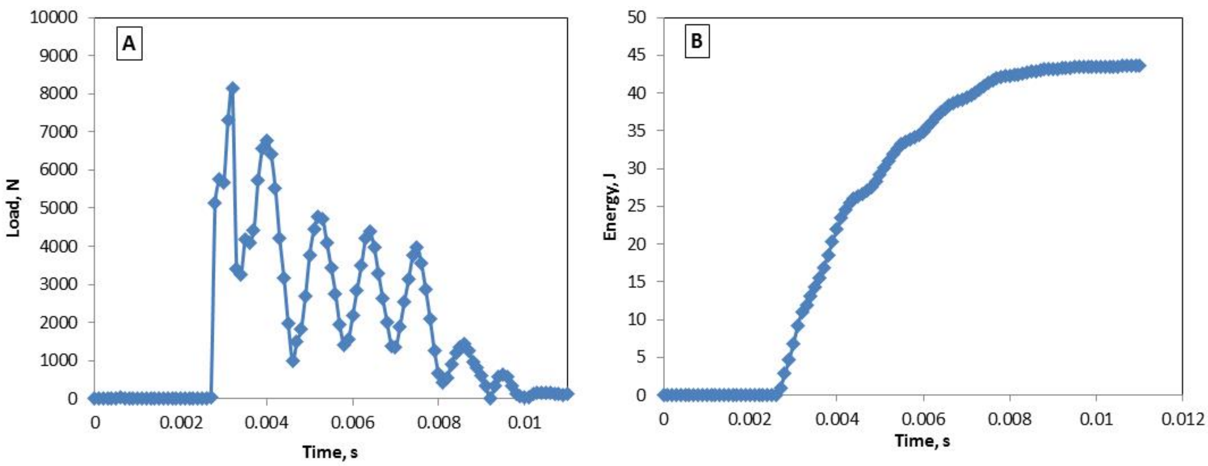

Figure 12. Typical impact load time-history (**A**) and cumulative impact energy absorption capacity (**B**) of UHPC.

The impact load–time history (see Figure 12A) exhibits a sharp rise in load immediately following contact, reaching peak levels within a few milliseconds. Peak impact loads on the order of several kilonewtons were recorded, followed by a sequence of load oscillations and gradual decay. These oscillations indicate repeated engagement and disengagement of internal load-transfer mechanisms, including crack formation, crack arrest, and fiber pull-out, rather than a single catastrophic failure event. The absence of an abrupt load drop after first contact suggests that the UHPC specimens retained structural integrity throughout the impact event.

The cumulative impact energy absorption curve reveals (see Figure 12B) that the majority of energy dissipation occurred over a short time interval following impact initiation, with energy absorption increasing rapidly during the first 3–6 ms. Beyond this interval, the rate of energy accumulation gradually diminished, approaching a plateau as damage mechanisms were exhausted and residual load-carrying capacity decreased. The total absorbed impact energy measured for the UHPC specimens was 42.97 J, with a 95% confidence interval of ±0.91 J. This narrow confidence interval corresponds to approximately 2% relative variability, indicating highly consistent impact performance across specimens.

From an energy perspective, the measured absorption capacity is several times greater than values typically reported for conventional concrete specimens of comparable dimensions, which often fail after absorbing only a few joules of energy. Even fiber-reinforced standard- or high-strength concretes exhibit impact energy absorption capacities well below 20 J under similar testing conditions [71]. The UHPC mixture investigated here, therefore, demonstrates an energy absorption capacity that exceeds that of conventional concrete by an order of magnitude and surpasses that of many fiber-reinforced systems, reflecting the combined influence of matrix densification and effective fiber engagement.

The shape of the cumulative energy curve provides further insight into the governing mechanisms. The smooth, monotonic increase in absorbed energy, without sudden drops or discontinuities, indicates that damage evolved in a stable manner rather than through unstable crack propagation. This behavior is consistent with progressive fiber pull-out and frictional sliding at the fiber–matrix interface, which dissipates energy over an extended displacement history. Matrix cracking alone cannot account for the observed energy levels, as the energy required to create new fracture surfaces in a brittle cementitious matrix is comparatively small. Instead, the dominant contribution arises from fiber-controlled mechanisms activated during rapid crack opening.

It is also worth mentioning that significant energy absorption occurred without complete perforation or fragmentation of the specimens. The UHPC plates' ability to remain largely intact after impact demonstrates a high degree of damage tolerance, particularly relevant for applications involving accidental or extreme loading scenarios. The retention of specimen integrity after absorbing more than 40 J of impact energy highlights the fiber network's effectiveness in redistributing stresses and preventing localized failure. When considered alongside the flexural and direct tensile results, the impact performance reinforces the interpretation of UHPC as a material governed by fracture resistance and energy dissipation rather than peak strength alone. The high impact energy absorption capacity is consistent with the observed ductile post-peak behavior in bending and the extended strain capacity under direct tension. Together, these results indicate that the UHPC mixture possesses a robust ability to accommodate rapid loading through distributed damage and controlled crack evolution.

4.7. Size and Geometry Effects on Compressive Strength

The influence of specimen size and geometry on the measured compressive strength of UHPC was evaluated using 50 and 75 mm cube specimens and 75 × 150 mm cylindrical specimens. The mean compressive strengths obtained at 7 and 28 days, together with the corresponding confidence intervals, are presented in Figure 13. The results indicate that specimen size has a measurable influence on the nominal compressive strength, with smaller specimens generally exhibiting higher strengths at both testing ages.

At 7 days, the mean compressive strengths of the 75 mm cubes, 50 mm cubes, and 75 × 150 mm cylinders were 201, 221, and 209 MPa, respectively. At 28 days, the corresponding strengths increased to approximately 213, 227, and 218 MPa. Thus, the 50 mm cubes exhibited the highest nominal compressive strength at both ages, whereas the 75 mm cubes exhibited the lowest strength. Relative to the 75 mm cubes, reducing the cube size from 75 to 50 mm increased the nominal compressive strength by approximately 10% at 7 days and 7% at 28 days. When compared with the 75 × 150 mm cylinders, the corresponding increases were approximately 6% and 4%, respectively. These results demonstrate that the influence of specimen size persisted at 28 days but was relatively modest.

The higher nominal strength obtained from the smaller 50 mm cubes can be attributed to statistical size effects and fracture-mechanics considerations. Smaller specimens have a lower probability of containing a critical flaw within the stressed volume and generally store less elastic energy at failure, which can result in higher nominal strengths [2,72]. As specimen dimensions increase, the probability of activating a critical defect increases, while the larger volume of stored elastic energy can promote crack propagation and failure at a lower nominal stress. The observed differences between the 50 and 75 mm cubes are therefore consistent with the expected size-dependent behavior of quasi-brittle cement-based materials.

https://doi.org/10.3390/sci8090248

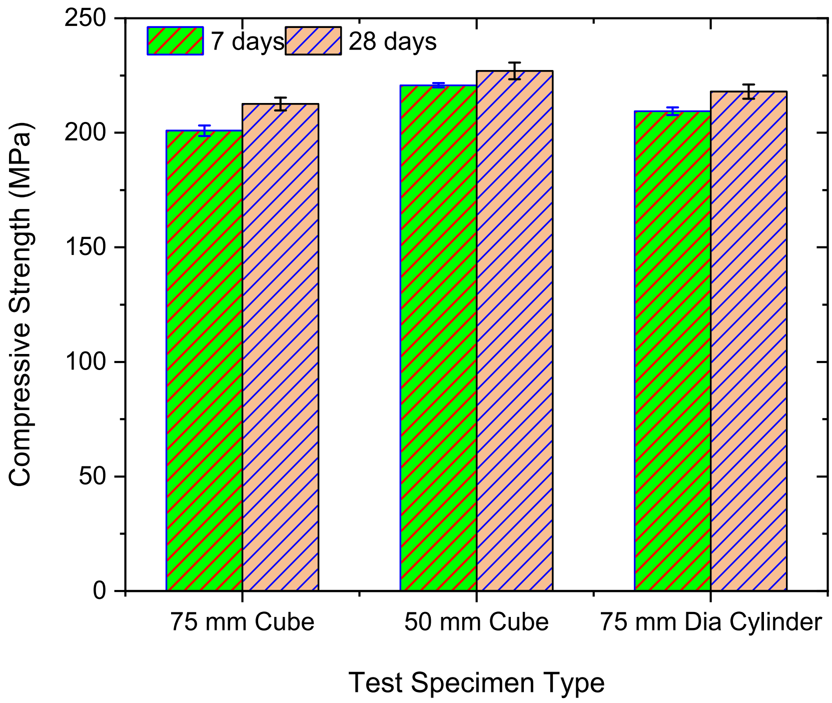

Figure 13. Mean compressive strength of UHPC measured using different specimen sizes and geometries at 7 and 28 days. Error bars represent the 95% confidence intervals.

The comparison between the 75 mm cubes and 75 × 150 mm cylinders provides additional insight into the influence of specimen geometry. At 7 days, the cylinder strength of approximately 209 MPa was slightly higher than the 201 MPa obtained from the 75 mm cubes, whereas at 28 days the corresponding values were approximately 218 and 213 MPa, respectively. The relatively small differences between these two specimen configurations suggest that, within the investigated range, specimen size has a more discernible influence on nominal strength than specimen shape. The confidence intervals shown in Figure 13 further indicate that the differences among the larger specimen configurations are relatively limited compared with the difference between the 50 and 75 mm cubes.

The magnitude of the observed size effect is smaller than the reductions commonly reported for conventional and high-strength concretes when specimen dimensions are increased [73]. This moderated size dependence may be associated with the enhanced fracture resistance of the steel fiber-reinforced UHPC. Fiber bridging can restrain crack opening, promote distributed microcracking, and dissipate fracture energy, thereby reducing the sensitivity of the material to specimen dimensions [16,24]. Nevertheless, the persistence of higher nominal strength in the smaller 50 mm cubes indicates that fiber reinforcement does not completely eliminate size-dependent behavior.

The relatively small increase in compressive strength from 7 to 28 days observed for all specimen configurations also indicates that the specimen-size effect was not substantially altered by age under the adopted curing regime. The increases from 7 to 28 days were approximately 6%, 3%, and 4% for the 75 mm cubes, 50 mm cubes, and 75 × 150 mm cylinders, respectively. This limited age-dependent strength development is consistent with the accelerated hydration and pozzolanic reactions promoted during the initial 48 h of steam curing, followed by conditioning at approximately 50% relative humidity, where the availability of external moisture for continued hydration is limited.

From a practical perspective, the results demonstrate the importance of specimen size and geometry when comparing UHPC compressive-strength data obtained using different testing configurations. The approximately 4% higher strength of the 50 mm cubes relative to the

75 × 150 mm cylinders at 28 days indicates that small cube specimens can produce somewhat higher nominal strengths than larger specimens. Although the magnitude of this difference is relatively limited for the investigated UHPC, it should be considered when comparing laboratory results obtained from different specimen configurations or when extrapolating laboratory-scale measurements to structural-scale applications. The 75 × 150 mm cylinder results are therefore retained as the principal compressive-strength values in this study, while the cube results provide useful evidence of the size and geometry effects exhibited by the investigated UHPC.

4.8. Ultrasound Pulse Velocity

The ultrasound pulse velocity (UPV) test results for UHPC and normal-strength concrete are presented in Figure 14. The UHPC specimens exhibit a pulse velocity of approximately 5344 m/s, whereas the normal-strength concrete specimens show a lower value of roughly 5145 m/s. This represents an increase in pulse velocity of about 200 m/s, corresponding to an improvement of approximately 4% for UHPC relative to normal-strength concrete.

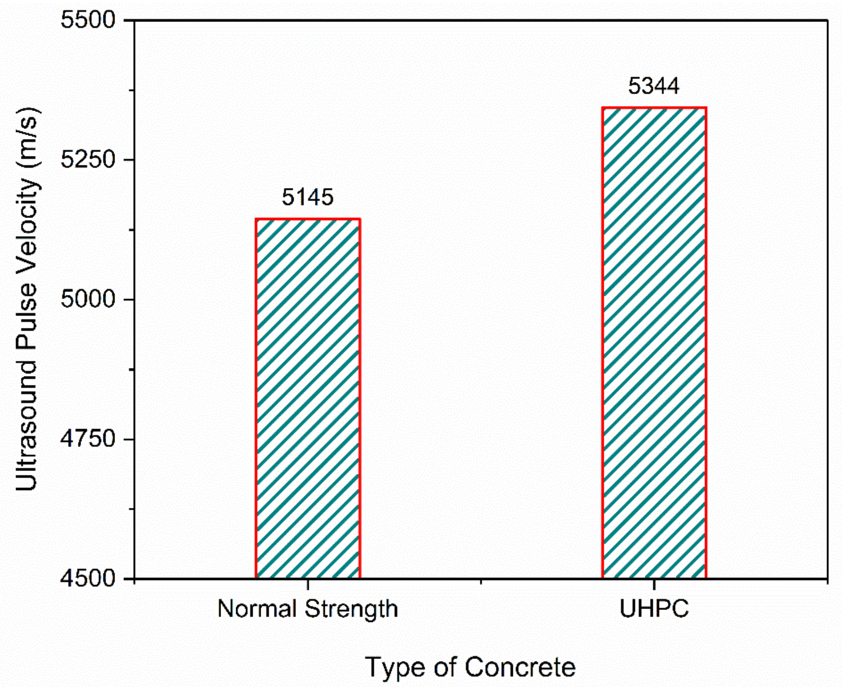

Figure 14. Ultrasound pulse velocity test results for UHPC and normal-strength concrete.

UPV is strongly influenced by material density, elastic stiffness, and internal continuity. The higher UPV measured for UHPC reflects its dense microstructure, reduced void content, and improved continuity of the solid phase. The high bulk density of UHPC, measured as 2.472 g/cm^3, contributes directly to faster wave propagation by reducing scattering and reflection of ultrasonic waves at pore boundaries [66].

In normal-strength concrete, a higher volume of capillary pores and weaker paste–aggregate interfaces introduce discontinuities that slow the transmission of ultrasonic waves. In contrast, the refined pore structure and dense particle packing of the adopted UHPC mixture provide a more homogeneous and continuous medium for wave propagation, resulting in higher measured pulse velocities [67].

The elevated UPV values measured for UHPC are consistent with its low water absorption capacity, low void content, and reduced sorptivity reported in other sections of this study [68]. Together, these results indicate a compact and well-integrated internal structure with limited internal defects. The UPV measurements, therefore, provide indirect confirmation of the dense matrix quality of UHPC and support the durability-related findings from transport and abrasion tests. The higher UPV of UHPC confirms its enhanced internal integrity compared with normal-strength concrete. It demonstrates the effectiveness of mixture design strategies aimed at producing a highly compact cementitious composite.

5. Integrated Mechanical Performance and Implications

The mechanical characterization presented in the preceding sections demonstrates that the UHPC mixture investigated in this study exhibits a consistent, interconnected set of strength, ductility, and energy dissipation characteristics that cannot be inferred from any single mechanical indicator in isolation. Instead, the observed behavior reflects the combined influence of matrix densification, fiber reinforcement, fracture resistance, and internal structural integrity across different loading modes and length scales.

The exceptionally high compressive strength of 220 MPa at an early age, indicates a dense and mechanically robust cementitious matrix. However, the significance of this compressive capacity becomes evident only when considered alongside the tensile and flexural responses. Direct tensile testing shows that the UHPC mixture sustains tensile stresses exceeding 10 MPa, with a measurable strain-hardening regime and extended deformation capacity. This tensile behavior provides the fundamental mechanism underpinning the ductile flexural response observed under bending, where load-carrying capacity is maintained well beyond first cracking through controlled crack opening and effective fiber bridging.

Although strain hardening was not observed in flexure, the presence of stable post-peak softening and substantial residual load capacity indicates that the material operates in a damage-tolerant regime rather than a brittle one. The difference between tensile and flexural responses highlights the role of stress state and crack kinematics in governing fiber engagement. Under uniaxial tension, the relatively uniform stress field promotes more effective mobilization of fiber bridging capacity, whereas under bending, stress gradients and crack localization limit the development of multiple cracking. This distinction underscores the importance of direct tensile testing for capturing the intrinsic tensile mechanics of UHPC.

The flexural, direct tensile, and impact responses should not be viewed as independent mechanical properties but rather as complementary manifestations of the same fracture-controlled behavior. Under direct tension, the initiation and propagation of cracks are resisted primarily through stress transfer across the crack plane by the steel fibers, resulting in strain hardening and enhanced deformation capacity. Under flexural loading, this same fiber-bridging mechanism delays crack localization, maintains residual load-carrying capacity after first cracking, and promotes stable post-peak softening. During impact loading, the fibers continue to bridge rapidly propagating cracks, dissipating a significant amount of energy through crack deflection, fiber pull-out, and interfacial friction. The consistent improvement observed in these three independent tests therefore demonstrates that the outstanding mechanical performance of the developed UHPC is governed principally by fracture resistance and controlled crack evolution rather than by compressive strength alone.

The split tensile results further bridge the gap between flexural and direct tensile behavior by demonstrating a substantial enhancement in indirect tensile resistance relative to normal-strength concrete and conventional fiber-reinforced systems. The elevated split tensile strength confirms that the fiber–matrix interaction is sufficiently strong to delay crack initiation and promote distributed cracking under tensile-dominated loading, even when the stress state is not purely uniaxial. Impact testing extends this mechanical narrative into the dynamic regime. The ability of the UHPC specimens to absorb more than 40 J of impact energy with low variability and without catastrophic fragmentation reflects the same underlying mechanisms observed under quasi-static loading: progressive cracking, fiber pull-out, and frictional energy dissipation. The smooth evolution of cumulative absorbed energy indicates stable damage development, reinforcing the interpretation that UHPC behavior is governed by fracture resistance and energy dissipation rather than peak strength alone.

Non-destructive ultrasound pulse velocity measurements provide a critical complementary perspective on this integrated mechanical performance. The higher UPV measured for UHPC compared with normal-strength concrete indicates a dense, well-integrated internal structure with reduced void content and improved solid-phase continuity. These characteristics are consistent with the low water absorption capacity, low sorptivity, and refined pore structure reported earlier, and they provide indirect confirmation that the mechanical response observed across different tests is not influenced by internal defects or material heterogeneity. In this context, UPV serves as a structural integrity indicator that supports the interpretation of the mechanical results, particularly when comparing specimens of different sizes and loading configurations.

Investigating size effects on compressive strength provides an additional perspective on the mechanical integrity of the UHPC system. While a measurable size dependence remains, its magnitude is significantly lower than that typically reported for conventional concretes. This moderated size effect is consistent with the enhanced fracture toughness imparted by fiber reinforcement, which limits crack localization and delays unstable fracture. At the same time, the persistence of a size effect confirms that UHPC behavior remains governed by fracture mechanics considerations at very high stress levels, particularly as specimen size increases and stored elastic energy becomes more influential.

These results indicate that the UHPC mixture developed in this study behaves as a structural composite in which strength, ductility, internal integrity, and energy dissipation are intrinsically linked. High compressive strength provides the foundation for the mechanical performance of UHPC; however, the flexural, direct tensile, and impact responses collectively demonstrate that the material's structural behavior is governed primarily by its ability to resist crack initiation, bridge propagating cracks, and dissipate fracture energy. Still, it is the tensile capacity, crack-bridging efficiency, fracture resistance, and dense internal structure that govern deformation capacity, damage tolerance, and response under both static and dynamic loading. The integrated mechanical and non-destructive assessment presented here supports the interpretation of UHPC as a material whose performance is controlled by stable crack evolution and internal continuity across multiple loading modes, rather than by compressive strength in isolation.

It should be noted that all test results reported in this study correspond to specimens tested at an age of 7 days following steam curing at 90 °C for 48 h. Under this curing regime, UHPC develops a substantial proportion of its ultimate mechanical properties owing to accelerated hydration and enhanced pozzolanic reactions. Consequently, although the present results were obtained at 7 days, they are broadly comparable with the 28-day properties of conventionally cured UHPC reported in the literature. Nevertheless, direct comparisons should take into account differences in curing regime, binder composition, and testing age.

It should also be noted that all specimens investigated in this study were produced from a single UHPC batch. Therefore, the reported statistical measures of variability reflect the repeatability of specimen preparation and testing within a single production batch rather than batch-to-batch reproducibility. Although the low variability demonstrates excellent consistency in the manufacturing, curing, and testing procedures adopted in this study, further investigation involving multiple independently produced batches would be required to assess the reproducibility and manufacturing robustness of the proposed UHPC mixture.

From a sustainability perspective, the UHPC mixture investigated in this study involves a relatively high binder content and an energy-intensive steam-curing regime, which may increase its environmental and economic footprint compared with conventional concrete. However, the superior mechanical performance and durability of UHPC can offset these impacts over the service life. While a detailed life-cycle assessment is beyond the scope of this study, the use of slag and limestone powder contributes toward improved sustainability, and further work is recommended to quantify these benefits.

6. Recommendations for Future Research

The results of this study provide a detailed mechanical characterization of steel fiber-reinforced UHPC under multiple loading modes; however, they also highlight several aspects of UHPC behavior that merit further investigation. In particular, the interactions among fiber reinforcement, fracture processes, and specimen scale remain only partially resolved. Addressing these aspects is essential for advancing the predictive understanding and structural application of UHPC beyond laboratory-scale testing.

1. Further investigation is warranted into the role of fiber reinforcement parameters, including volume fraction, aspect ratio, and orientation distribution, on the transition between strain-softening and strain-hardening behavior under flexural loading. In particular, systematic variation in fiber characteristics under identical matrix composition would help clarify the conditions required to achieve multiple cracking in bending while preserving the high compressive strength observed in this study.
2. Multi-scale fracture characterization, combining direct tensile testing with acoustic emission monitoring or digital image correlation, could provide deeper insight into crack initiation, crack spacing, and fiber engagement during loading. Such approaches would enable quantitative correlation between macroscopic stress–strain response and underlying damage mechanisms in UHPC.
3. The influence of specimen size and geometry on tensile and flexural behavior remains less well understood than that of compressive strength. Extending size-effect investigations to direct tension and bending would improve the reliability of extrapolating laboratory-scale ductility and toughness measurements to structural-scale UHPC elements.
4. Given the strong impact energy absorption capacity observed, future studies should examine the strain-rate sensitivity of UHPC under intermediate and high loading rates. Controlled dynamic tensile and flexural tests would help determine whether the ductile mechanisms identified under quasi-static conditions remain effective under more severe impact or blast-type loading.

7. Conclusions

This study investigated the mechanical performance of steel fiber-reinforced UHPC under quasi-static and dynamic loading. The key findings are summarized as follows:

(1) The investigated UHPC achieved high compressive strength, with mean values of approximately 209 and 218 MPa at 7 and 28 days, respectively, in 75 × 150 mm cylindrical specimens. The relatively modest increase of approximately 4% from 7 to 28 days indicates that most strength development occurred during the initial 48 h steam-curing period. The high compressive strength is attributed to the low water-to-binder ratio, high cementitious content, dense particle packing, incorporation of supplementary cementitious materials, and steam-curing regime.

(2) The material exhibited enhanced tensile and flexural performance, with flexural strength of approximately 33 MPa, split tensile strength of about 16 MPa, and direct tensile strength exceeding 10 MPa with strain capacities of 0.25–0.30%, indicating pronounced ductility, controlled crack propagation, and efficient fiber bridging mechanisms.

(3) Impact resistance was significantly improved, with absorbed energy exceeding 40 J and stable damage progression governed primarily by fiber pull-out and interfacial friction, reflecting the ability of the composite to dissipate energy under dynamic loading conditions.

(4) A measurable but limited specimen-size and geometry effect was observed in compressive strength. The 50 mm cubes produced higher nominal strengths than the 75 mm cubes and 75 × 150 mm cylinders at both 7 and 28 days, with the 50 mm cubes reaching approximately 221 and 227 MPa, respectively. At 28 days, the difference between the 50 mm cubes and 75 × 150 mm cylinders was approximately 4%, indicating that steel fiber reinforcement may moderate, but does not eliminate, size-dependent behavior.

(5) Non-destructive and physical measurements (UPV ≈ 5344 m/s, high density, low porosity, and low water absorption) confirmed the dense and homogeneous microstructure, which is consistent with the observed improvements in mechanical strength, durability-related properties, and overall material integrity.

Overall, the investigated steam-cured UHPC mixture exhibited a combination of high compressive strength, tensile and flexural capacity, and impact resistance, with steel fiber bridging playing an important role in crack control and energy dissipation. The findings are specific to the investigated matrix composition, fiber reinforcement, specimen configurations, and curing regime. Further studies involving additional matrix compositions, curing conditions, larger standard and structural-scale specimens, and long-term mechanical performance are warranted to establish the broader applicability of the findings.

Author Contributions: Conceptualization, A.B., Y.C., S.R., A.B.-J., R.-U.-D.N. and P.S.; methodology, A.B., Y.C., S.R., A.B.-J. and R.-U.-D.N.; formal analysis, A.B., Y.C., S.R., A.B.-J. and R.-U.-D.N.; investigation, A.B., Y.C., S.R., A.B.-J. and R.-U.-D.N.; data curation, A.B., Y.C., S.R., A.B.-J. and R.-U.-D.N.; writing—original draft preparation, R.-U.-D.N., A.B.-J. and P.S.; writing—review and editing, A.B., Y.C., S.R., A.B.-J., R.-U.-D.N. and P.S. All authors have read and agreed to the published version of the manuscript.

Funding: This research was supported by the U.S. Air Force through Grant No. FA9550-15-C-0012.

Data Availability Statement: The original contributions presented in this study are included in the article. Further inquiries can be directed to the corresponding authors.

Acknowledgments: The financial support provided by the U.S. Air Force for this work is thankfully acknowledged.

Conflicts of Interest: The authors declare that they have no financial or non-financial interests that are directly or indirectly related to this work.

References

1. Sha, H.; Chong, X.; Li, J.; Gao, J.; Huang, J.; Zhan, B. A uniaxial tensile constitutive model for ultra-high performance concrete considering fiber volume fraction and orientation. *J. Build. Eng.* **2025**, *113*, 114003. [CrossRef]
2. Ouyang, X.; Wu, Z.; Shan, B.; Chen, Q.; Shi, C. A critical review on compressive behavior and empirical constitutive models of concrete. *Constr. Build. Mater.* **2022**, *323*, 126572. [CrossRef]
3. Simanjuntak, R.P.; Aslani, F. Constitutive relationships for ultra-high-performance concrete at elevated temperatures. *Sci. Rep.* **2025**, *15*, 4957. [CrossRef] [PubMed]
4. Zhang, D.; Tan, G.Y.; Tan, K.H. Combined effect of flax fibers and steel fibers on spalling resistance of ultra-high performance concrete at high temperature. *Cem. Concr. Compos.* **2021**, *121*, 104067. [CrossRef]
5. Yoo, D.-Y.; Kim, S.-W.; Park, J.-J. Comparative flexural behavior of ultra-high-performance concrete reinforced with hybrid straight steel fibers. *Constr. Build. Mater.* **2017**, *132*, 219–229. [CrossRef]

6. Yu, R.; Spiesz, P.; Brouwers, H.J.H. Development of Ultra-High Performance Fibre Reinforced Concrete (UHPFRC): Towards an efficient utilization of binders and fibres. *Constr. Build. Mater.* **2015**, *79*, 273–282. [CrossRef]
7. Ren, G.; Yao, B.; Ren, M.; Gao, X. Utilization of natural sisal fibers to manufacture eco-friendly ultra-high performance concrete with low autogenous shrinkage. *J. Clean. Prod.* **2022**, *332*, 130105. [CrossRef]
8. You, I.; Lee, Y.; Yoo, D.-Y.; Zi, G. Influence of liquid crystal display glass powder on the tensile performance of ultra-high-performance fiber-reinforced concrete. *J. Build. Eng.* **2022**, *57*, 104901. [CrossRef]
9. Cao, X.; Ren, Y.-C.; Qian, K.; Fu, F.; Deng, X.F.; Zhang, W.J. Size effect on flexural behavior of ultra-high-performance concrete beams with different reinforcement. *Structures* **2022**, *41*, 969–981. [CrossRef]
10. Sun, M.; Yu, R.; Jiang, C.; Fan, D.; Shui, Z. Quantitative effect of seawater on the hydration kinetics and microstructure development of Ultra High Performance Concrete (UHPC). *Constr. Build. Mater.* **2022**, *340*, 127733. [CrossRef]
11. Rui, Y.; Kangning, L.; Tianyi, Y.; Liwen, T.; Mengxi, D.; Zhonghe, S. Comparative study on the effect of steel and polyoxymethylene fibers on the characteristics of Ultra-High Performance Concrete (UHPC). *Cem. Concr. Compos.* **2022**, *127*, 104418. [CrossRef]
12. Stengel, T.; Schießl, P. 22—Life cycle assessment (LCA) of ultra high performance concrete (UHPC) structures. In *Eco-Efficient Construction and Building Materials*; Pacheco-Torgal, F., Cabeza, L.F., Labrincha, J., de Magalhães, A., Eds.; Woodhead Publishing: Cambridge, UK, 2014; pp. 528–564.
13. Thomas, R.J.; Sorensen, A.D. Review of strain rate effects for UHPC in tension. *Constr. Build. Mater.* **2017**, *153*, 846–856. [CrossRef]
14. Hassan, M.; Wille, K. Experimental impact analysis on ultra-high performance concrete (UHPC) for achieving stress equilibrium (SE) and constant strain rate (CSR) in Split Hopkinson pressure bar (SHPB) using pulse shaping technique. *Constr. Build. Mater.* **2017**, *144*, 747–757. [CrossRef]
15. Rossi, P. Influence of fibre geometry and matrix maturity on the mechanical performance of ultra high-performance cement-based composites. *Cem. Concr. Compos.* **2017**, *37*, 246–248. [CrossRef]
16. Mahmud, G.H.; Yang, Z.; Hassan, A.M.T. Experimental and numerical studies of size effects of Ultra High Performance Steel Fibre Reinforced Concrete (UHPFRC) beams. *Constr. Build. Mater.* **2013**, *48*, 1027–1034. [CrossRef]
17. Zhang, Y.; Zhu, Y.; Qu, S.; Kumar, A.; Shao, X. Improvement of flexural and tensile strength of layered-casting UHPC with aligned steel fibers. *Constr. Build. Mater.* **2020**, *251*, 118893. [CrossRef]
18. Zhang, Y.; Yang, J.; Li, T.; Deng, M. Mechanical behavior of RC columns strengthened with thin UHPC jacket under cyclic loads. *J. Build. Eng.* **2022**, *49*, 104065. [CrossRef]
19. Wille, K.; El-Tawil, S.; Naaman, A.E. Properties of strain hardening ultra high performance fiber reinforced concrete (UHP-FRC) under direct tensile loading. *Cem. Concr. Compos.* **2014**, *48*, 53–66. [CrossRef]
20. Ma, K.; Cao, X.; Song, J.; Meng, X.; Qiao, L. Axial compressive behavior of concrete-filled steel tubes with GFRP-confined UHPC cores. *J. Constr. Steel Res.* **2023**, *200*, 107632. [CrossRef]
21. Wu, H.; Zang, Z.; Deng, S.; Shen, A.; Cai, Y.; Ren, G.; Pan, H. Recent developments in pullout behaviors and tensile properties of ultra-high-performance concrete reinforced with steel fiber. *Arch. Civ. Mech. Eng.* **2023**, *23*, 216. [CrossRef]
22. Hossain, M.A.; Datta, S.D.; Akid, A.S.M.; Sobuz, M.H.; Islam, M.S. Exploring the synergistic effect of fly ash and jute fiber on the fresh, mechanical and non-destructive characteristics of sustainable concrete. *Heliyon* **2023**, *9*, e21708. [CrossRef] [PubMed]
23. Tan, Y.; Yu, H.; Mi, R.; Zhang, Y. Compressive strength evaluation of coral aggregate seawater concrete (CAC) by non-destructive techniques. *Eng. Struct.* **2018**, *176*, 293–302. [CrossRef]
24. Zhang, S.S.; Wang, J.J.; Lin, G.; Yu, T.; Fernando, D. Stress-strain models for ultra-high performance concrete (UHPC) and ultra-high performance fiber-reinforced concrete (UHPFRC) under triaxial compression. *Constr. Build. Mater.* **2023**, *370*, 130658. [CrossRef]
25. Abdellatief, M.; Elrahman, M.A.; Elgendy, G.; Bassioni, G.; Tahwia, A.M. Response surface methodology-based modelling and optimization of sustainable UHPC containing ultrafine fly ash and metakaolin. *Constr. Build. Mater.* **2023**, *388*, 131696. [CrossRef]
26. Wen, C.; Zhang, P.; Wang, J.; Hu, S. Influence of fibers on the mechanical properties and durability of ultra-high-performance concrete: A review. *J. Build. Eng.* **2022**, *52*, 104370. [CrossRef]
27. Le Hoang, A.; Fehling, E. Influence of steel fiber content and aspect ratio on the uniaxial tensile and compressive behavior of ultra high performance concrete. *Constr. Build. Mater.* **2017**, *153*, 790–806. [CrossRef]
28. McSwain, A.C.; Berube, K.A.; Cusatis, G.; Landis, E.N. Confinement effects on fiber pullout forces for ultra-high-performance concrete. *Cem. Concr. Compos.* **2018**, *91*, 53–58. [CrossRef]
29. *ASTM C642-21*; Standard Test Method for Density, Absorption, and Voids in Hardened Concrete. ASTM International: West Conshohocken, PA, USA, 2022.
30. *ASTM C78/C78M-22*; Standard Test Method for Flexural Strength of Concrete (Using Simple Beam with Third-Point Loading). ASTM International: West Conshohocken, PA, USA, 2022.
31. *ASTM C496/C496M-17*; Standard Test Method for Splitting Tensile Strength of Cylindrical Concrete Specimens. ASTM International: West Conshohocken, PA, USA, 2017.

32. *ASTM D7136*; Standard Test Method for Measuring the Damage Resistance of a Fiber-Reinforced Polymer Matrix Composite to a Drop-Weight Impact Event. ASTM International: West Conshohocken, PA, USA, 2015.
33. Gesoglu, M.; Güneyisi, E.; Muhyaddin, G.F.; Asaad, D.S. Strain hardening ultra-high performance fiber reinforced cementitious composites: Effect of fiber type and concentration. *Compos. Part B Eng.* **2016**, *103*, 74–83. [CrossRef]
34. Abadel, A.; Abbas, H.; Albidah, A.; Almusallam, T.; Al-Salloum, Y. Effectiveness of GFRP strengthening of normal and high strength fiber reinforced concrete after exposure to heating and cooling. *Eng. Sci. Technol. Int. J.* **2022**, *36*, 101147. [CrossRef]
35. Hari, R.; Mini, K.M. Mechanical and durability properties of sisal-Nylon 6 hybrid fibre reinforced high strength SCC. *Constr. Build. Mater.* **2019**, *204*, 479–491. [CrossRef]
36. Abd-Elrahman, M.H.; Saad Agwa, I.; Mostafa, S.A.; Youssf, O. Effect of utilizing peanut husk ash on the properties of ultra-high strength concrete. *Constr. Build. Mater.* **2023**, *384*, 131398. [CrossRef]
37. Li, Y.; Tan, K.H.; Yang, E.-H. Influence of aggregate size and inclusion of polypropylene and steel fibers on the hot permeability of ultra-high performance concrete (UHPC) at elevated temperature. *Constr. Build. Mater.* **2018**, *169*, 629–637. [CrossRef]
38. Bermudez, M.; Wen, K.-W.; Hung, C.-C. A Comparative Study on the Shear Behavior of UHPC Beams with Macro Hooked-End Steel Fibers and PVA Fibers. *Materials* **2022**, *15*, 1485. [CrossRef] [PubMed]
39. Ghafari, E.; Costa, H.; Júlio, E. RSM-based model to predict the performance of self-compacting UHPC reinforced with hybrid steel micro-fibers. *Constr. Build. Mater.* **2014**, *66*, 375–383. [CrossRef]
40. Li, W.; Lu, Y.; Wang, P.; Jiang, Y.; Wang, L.; Shi, T.; Zheng, K. Comparative study of compressive behavior of confined NSC and UHPC/UHPFRC cylinders externally wrapped with CFRP jacket. *Eng. Struct.* **2023**, *292*, 116513. [CrossRef]
41. Zhang, T.; Zhang, M.; Shen, Y.; Zhu, H.; Yan, Z. Mitigating the damage of ultra-high performance concrete at elevated temperatures using synergistic flame-retardant polymer fibres. *Cem. Concr. Res.* **2022**, *158*, 106835. [CrossRef]
42. Kim, J.J.; Reda Taha, M. Experimental and Numerical Evaluation of Direct Tension Test for Cylindrical Concrete Specimens. *Adv. Civ. Eng.* **2014**, *2014*, 156926. [CrossRef]
43. Sastry, M.R.L.; Karumuri, S.R.; Rao, P. Considerations in Producing High Performance Concrete and Comparison of Concrete Mix Design Methods. *IUP J. Struct. Eng.* **2011**, *4*, 37.
44. Wille, K.; Naaman, A.E.; Parra-Montesinos, G.J. Ultra-High Performance Concrete with Compressive Strength Exceeding 150 MPa (22 ksi): A Simpler Way. *Aci. Mater. J.* **2011**, *108*, 46–54. [CrossRef]
45. Prem, P.; Bharatkumar, B.; Iyer, N. Mechanical properties of ultra high performance concrete. *World Acad. Sci. Eng. Technol.* **2012**, *8*, 676–685.
46. Yoo, D.-Y.; Kim, J.-J.; Chun, B. Dynamic pullout behavior of half-hooked and twisted steel fibers in ultra-high-performance concrete containing expansive agents. *Compos. Part B Eng.* **2019**, *167*, 517–532. [CrossRef]
47. Huang, H.; Gao, X.; Khayat, K.H. Contribution of fiber alignment on flexural properties of UHPC and prediction using the Composite Theory. *Cem. Concr. Compos.* **2021**, *118*, 103971. [CrossRef]
48. Xiang, D.; Hou, Z.; Liu, Y.; Li, Y.; Xu, X. Flexural behavior and crack width prediction of UHPC slabs reinforced with FRP bars. *J. Build. Eng.* **2023**, *77*, 107548. [CrossRef]
49. Xiao, J.; Zhou, M.; Nie, J.-G.; Yang, T.Y.; Fan, J.S. Flexural behavior of steel-UHPC composite slabs with perfobond rib shear connectors. *Eng. Struct.* **2021**, *245*, 112912. [CrossRef]
50. Wu, Z.; Shi, C.; He, W.; Wang, D. Static and dynamic compressive properties of ultra-high performance concrete (UHPC) with hybrid steel fiber reinforcements. *Cem. Concr. Compos.* **2017**, *79*, 148–157. [CrossRef]
51. Shi, J.; Pan, W.; Kang, J.; Yu, Z.; Sun, G.; Li, J.; Zheng, K.; Shen, J. Properties of Ultra-High Performance Concrete incorporating iron tailings powder and iron tailings sand. *J. Build. Eng.* **2024**, *83*, 108442. [CrossRef]
52. Meng, W.; Khayat, K. Effect of hybrid fibers on fresh, mechanical properties, and autogenous shrinkage of cost effective UHPC. *J. Mater. Civ. Eng.* **2018**, *30*, 04018030. [CrossRef]
53. Meng, W.; Valipour, M.; Khayat, K.H. Optimization and performance of cost-effective ultra-high performance concrete. *Mater. Struct.* **2016**, *50*, 29. [CrossRef]
54. Milasi, S.E.; Mostofinejad, D.; Bahmani, H. Improving the resistance of ultra-high-performance concrete against nuclear radiation: Replacing cement with barite, hematite, and lead powder. *Dev. Built Environ.* **2023**, *15*, 100190. [CrossRef]
55. Namdar, A.; Zakaria, I.; Hazeli, A.; Azimi, S.J.; Razak, A.S.; Gopalakrishna, G.S. An experimental study on flexural strength enhancement of concrete by means of small steel fibers. *Frat. Ed. Integrità Strutt.* **2013**, *7*, 22–30. [CrossRef]
56. Aziz, O.; Ahmed, G. Mechanical Properties of Ultra High Performance Concrete (UHPC). *Spec. Publ.* **2012**, *289*, 1–16. [CrossRef]
57. Yoo, D.-Y.; Sohn, H.-K.; Borges, P.H.R.; Fediuk, R.; Kim, S. Enhancing the tensile performance of ultra-high-performance concrete through strategic use of novel half-hooked steel fibers. *J. Mater. Res. Technol.* **2020**, *9*, 2914–2925. [CrossRef]
58. Shi, Z.; Su, Q.; Kavoura, F.; Veljkovic, M. Uniaxial tensile response and tensile constitutive model of ultra-high performance concrete containing coarse aggregate (CA-UHPC). *Cem. Concr. Compos.* **2023**, *136*, 104878. [CrossRef]
59. Garas, V.Y.; Kahn, L.F.; Kurtis, K.E. Short-term tensile creep and shrinkage of ultra-high performance concrete. *Cem. Concr. Compos.* **2009**, *31*, 147–152. [CrossRef]

60. Hung, C.-C.; Chen, Y.-T.; Yen, C.-H. Workability, fiber distribution, and mechanical properties of UHPC with hooked end steel macro-fibers. *Constr. Build. Mater.* **2020**, *260*, 119944. [CrossRef]
61. Wille, K.; Naaman, A.E.; El-Tawil, S.; Parra-Montesinos, G.J. Ultra-high performance concrete and fiber reinforced concrete: Achieving strength and ductility without heat curing. *Mater. Struct.* **2012**, *45*, 309–324. [CrossRef]
62. Amran, M.; Huang, S.-S.; Onaizi, A.M.; Makul, N.; Abdelgader, H.S.; Ozbakkaloglu, T. Recent trends in ultra-high performance concrete (UHPC): Current status, challenges, and future prospects. *Constr. Build. Mater.* **2022**, *352*, 129029. [CrossRef]
63. Song, P.S.; Hwang, S. Mechanical properties of high-strength steel fiber-reinforced concrete. *Constr. Build. Mater.* **2004**, *18*, 669–673. [CrossRef]
64. Li, Q.-H.; Zhao, S.-Y.; Huang, B.-T.; Xu, L.Y.; Xu, S.L. Simultaneous enhancement of ductility and sustainability of high-strength Strain-Hardening Cementitious Composites (SHCC) using recycled fine aggregates. *J. Clean. Prod.* **2024**, *470*, 143357. [CrossRef]
65. Yang, J.; Chen, B.; Su, J.; Xu, G.; Zhang, D.; Zhou, J. Effects of fibers on the mechanical properties of UHPC: A review. *J. Traffic Transp. Eng.* **2022**, *9*, 363–387. [CrossRef]
66. Huang, B.-T.; Weng, K.-F.; Zhu, J.-X.; Xiang, Y.; Dai, J.G.; Li, V.C. Engineered/strain-hardening cementitious composites (ECC/SHCC) with an ultra-high compressive strength over 210 MPa. *Compos. Commun.* **2021**, *26*, 100775. [CrossRef]
67. Meng, L.; Zhang, C.; Wei, J.; Li, L.; Liu, J.; Wang, S.; Ding, Y. Mechanical properties and microstructure of ultra-high strength concrete with lightweight aggregate. *Case Stud. Constr. Mater.* **2023**, *18*, e01745. [CrossRef]
68. Buttignol, T.; Sousa, J.; Bittencourt, T. Ultra High-Performance Fiber-Reinforced Concrete (UHPFRC): A review of material properties and design procedures. *Ibracon Struct. Mater. J.* **2017**, *10*, 957–971. [CrossRef]
69. Yoo, D.-Y.; Kang, S.-T.; Yoon, Y.-S. Effect of fiber length and placement method on flexural behavior, tension-softening curve, and fiber distribution characteristics of UHPFRC. *Constr. Build. Mater.* **2014**, *64*, 67–81. [CrossRef]
70. Huang, Y.; Grünewald, S.; Schlangen, E.; Luković, M. Strengthening of concrete structures with ultra high performance fiber reinforced concrete (UHPFRC): A critical review. *Constr. Build. Mater.* **2022**, *336*, 127398. [CrossRef]
71. Yuan, C.; Yong, L.; Ziao, C.; Tianyi, Y.; Rui, Y. Development of Ultra-High Performance Concrete (UHPC) matrix based on recycled concrete fines subjected to coupling curing of microwave and wet carbonation. *J. Build. Eng.* **2024**, *95*, 110038. [CrossRef]
72. Yang, X.; Zhang, B.; Zhou, A.; Wei, H.; Liu, T. Axial compressive behaviour of corroded steel reinforced concrete columns retrofitted with a basalt fibre reinforced polymer-ultrahigh performance concrete jacket. *Compos. Struct.* **2023**, *304*, 116447. [CrossRef]
73. Kim, M.-J.; Yoo, D.-Y.; Kim, S.; Shin, M.; Banthia, N. Effects of fiber geometry and cryogenic condition on mechanical properties of ultra-high-performance fiber-reinforced concrete. *Cem. Concr. Res.* **2018**, *107*, 30–40. [CrossRef]